Development of a detailed gaseous oxidation scheme of naphthalene for secondary organic aerosol (SOA) formation and speciation

Victor Lannuque, Karine Sartelet

Atmos. Chem. Phys., 24, 8589–8606, 2024
https://doi.org/10.5194/acp-24-8589-2024

Atmospheric Chemistry and Physics
Open Access
EGU

Development of a detailed gaseous oxidation scheme of naphthalene for secondary organic aerosol (SOA) formation and speciation

Victor Lannuque[1,2] **and Karine Sartelet**[1]

[1]CEREA, École des Ponts ParisTech, EDF R&D, IPSL, 77455 Marne-la-Vallée, France
[2]National Institute for Industrial Environment and Risks (INERIS), 60550 Verneuil-en-Halatte, France

Correspondence: Victor Lannuque (victor.lannuque@ineris.fr)

Received: 8 March 2024 – Discussion started: 13 March 2024
Revised: 22 May 2024 – Accepted: 18 June 2024 – Published: 2 August 2024

Abstract. Naphthalene is the most abundant polycyclic aromatic hydrocarbon (PAH) in vehicle emissions and polluted urban areas. Its atmospheric oxidation products are oxygenated compounds that are potentially harmful for health and/or contribute to secondary organic aerosol (SOA) formation. Despite its impact on air quality, its complex structure and a lack of data mean that no detailed scheme of naphthalene gaseous oxidation for SOA formation and speciation has been established yet. This study presents the construction of the first near-explicit chemical scheme for naphthalene oxidation by OH, including kinetic and mechanistic data. The scheme redundantly represents all the classical steps of atmospheric organic chemistry (i.e., oxidation of stable species, peroxy radical formation and reaction, and alkoxy radical evolution), thus integrating fragmentation or functionalization pathways and the influence of NO_x on secondary compound formation. Missing kinetic and mechanistic data were estimated using structure–activity relationships (SARs) or by analogy with existing experimental or theoretical data. The proposed chemical scheme involves 383 species (231 stable species, including 93 % of the major molar masses observed in previous experimental studies) and 484 reactions with products. A first simulation reproducing experimental oxidation in an oxidation flow reactor under high-NO_x conditions shows a simulated SOA mass on the same order of magnitude as has been observed experimentally, with an error of −9 %.

1 Introduction

Organic aerosol (OA), and more specifically its secondary fraction, represents a significant proportion of all fine atmospheric particles (Gelencsér et al., 2007; Jimenez et al., 2009; Kroll and Seinfeld, 2008; Seinfeld and Pankow, 2003; Zhang et al., 2007). These particles affect air quality by impacting human health (Lim et al., 2018, 2012; Malley et al., 2017) and affect climate (Boucher et al., 2013). Secondary organic aerosol (SOA) is formed mainly via the condensation of low-volatility and/or water-soluble organic vapors produced by gas-phase oxidation (Seigneur, 2019).

The main precursors of anthropogenic SOAs are volatile monoaromatic compounds such as toluene or xylenes (Calvert et al., 2002; Hallquist et al., 2009; Henze et al., 2008) but also less-volatile compounds (Robinson et al., 2007) such as alkanes and polycyclic aromatic hydrocarbons (PAHs; Chen et al., 2016; Wang et al., 2018; Yuan et al., 2013). These PAHs are mainly emitted into the atmosphere during the incomplete combustion of fossil fuels or biomass (Baek et al., 1991; Boström et al., 2002; Mastral and Callén, 2000; Ravindra et al., 2008; Schauer et al., 1999a, b, 2001, 2002a, b). Their oxidation can lead to the formation of highly oxygenated compounds with low volatility (Atkinson et al., 1989; Atkinson and Arey, 2007; Bunce et al., 1997; Mihele et al., 2002; Wang et al., 2007). Whether in the gaseous or particulate phase, many PAHs and particularly nitroPAHs are recognized as potentially toxic, carcinogenic or mutagenic (Gupta et al., 1996; Helmig et al., 1992b, a; Josephy and Mannervik, 2006; Sasaki et al., 1995; Tokiwa et al., 1986).

Naphthalene is the most abundant PAH in vehicle emissions and polluted urban areas (Arey et al., 1967, 1989; Ens-

berg et al., 2014; Keyte et al., 2016; Martinet et al., 2017; Muñoz et al., 2018). Its oxidation products are often (i) less volatile and/or more water-soluble and therefore have greater aerosol-forming potential and (ii) more harmful to health than their precursors (Durant et al., 1998; Sasaki et al., 1997). To quantify the impact of atmospheric naphthalene on health, it is essential to understand and represent its gaseous oxidation chemical scheme in detail.

In air quality models, the oxidation of naphthalene (and other PAHs) and the subsequent formation of SOA are rarely represented or are only represented in a very simplified way, with just a few compounds (Appel et al., 2017; Majdi et al., 2019). Due to their complex structures and a lack of data, near-explicit chemical schemes such as from the Master Chemical Mechanism (MCM; Bloss et al., 2005; Jenkin et al., 2003) or those of the Generator for Explicit Chemistry and Kinetics of Organics in the Atmosphere (GECKO-A; Aumont et al., 2005) do not address PAH oxidation. The major products of naphthalene oxidation present in the gaseous and particulate phases have been identified during experimental studies, and formation pathways have been proposed for some of these products (Chan et al., 2009; Edwards et al., 2022; Kautzman et al., 2010). Other experimental or theoretical studies have proposed stoichiometry and kinetics for the reactions of naphthalene with different oxidants (Atkinson et al., 1984; Phousongphouang and Arey, 2002; Roueintan et al., 2014; Shiroudi et al., 2014). However, to our knowledge, no detailed gaseous oxidation scheme for naphthalene, combining kinetic and mechanistic data, has been established yet.

The aim of this study is to propose a detailed scheme of naphthalene gaseous oxidation for SOA formation. The development of the chemical scheme is based on (i) experimentally identified major oxidation products, (ii) proposed reaction pathways from the literature, (iii) theoretically and experimentally established kinetic data, and (iv) estimation of missing data using structure–activity relationships (SAR). The general method of scheme development is detailed in Sect. 2, the mechanism is described in Sect. 3, and it is evaluated in Sect. 4.

2 Scheme development general method

This section summarizes the main ideas and methodology behind the scheme construction. The details of each sub-part of the scheme are presented in Sect. 3. The complete chemical scheme and the lists of stable and radical species are available in the Supplement. The scheme has been developed with a view to (i) reproduce the molar masses (MW) observed during the naphthalene oxidation experiments described in the literature (Edwards et al., 2022; Kautzman et al., 2010) and (ii) follow the redundant architecture of atmospheric chemistry, making automatic generation possible.

While it is currently impossible to generate the chemical scheme for naphthalene oxidation using GECKO-A (which is limited to aliphatic and monoaromatic species), a similar redundant writing logic has been applied to write the new detailed scheme (see Aumont et al., 2005). The general mechanism thus follows the four steps listed below:

- reaction of a stable compound with an oxidant to form a carbon-centered radical or the occurrence of photolysis;
- addition of O_2 to form a peroxy radical (RO_2) or of NO_2 to form a nitro compound;
- potential reaction of RO_2 with NO, NO_2, NO_3, HO_2, or another RO_2 or via an autoxidation process to form a stable species, an alkoxy radical (RO), or a new RO_2 (via further addition of O_2); and
- RO decomposition, isomerization, or reaction with O_2 to form a stable compound and/or a new radical.

For PAHs, kinetics data are adapted from experimental data. Mechanistically, in the absence of precise data, we considered chemical transformations applying to one of the two cycles as having no impact on the second one. This has several implications:

- the two carbon atoms common to both rings (i.e., non-free) cannot be the site of oxidative attack as long as two aromatic rings are present;
- the addition of alcohol functions, which tends to increase the reactivity of the aromatic ring, or the addition of -nitro functions, which tends to decrease it, only modifies the reactivity of the aromatic ring on which it is located; and
- for PAHs with a peroxy radical (-OO•) group, the formation of a new ring with a peroxy bridge can only take place on free carbon atoms on the same aromatic ring.

Concerning the monoaromatic or aliphatic compounds in the chemical scheme, their chemistry is similar to that proposed by MCM or GECKO-A, with a few modifications based on experimental observations. Unless otherwise specified, kinetics and branching ratios of the reactions of these compounds with OH are estimated using the SARs and reaction data implemented in GECKO-A (Jenkin et al., 2018b, a). No stable species reactions with O_3 are considered. The kinetics of stable species reactions with NO_3 are estimated using the SAR from Kerdouci et al. (2014, 2010). Unless otherwise specified, the kinetics and branching ratios of RO_2 reactions are estimated using the SAR from Jenkin et al. (2019) as implemented in GECKO-A. For alkoxy radicals, kinetics are estimated using the SAR from (i) Vereecken and Peeters (2009) for decomposition, (ii) Vereecken and Peeters (2010) for H-migration, and (iii) Atkinson (2007) for the reactions with O_2. When the alkoxy radical function is on an aromatic ring, the compound can react with O_3, NO_2 or HO_2 following kinetics adapted from the works of Tao and Li (1999),

Platz et al. (1998), or Mousavipour and Homayoon (2011), as presented in Jenkin et al. (2018b). A rate coefficient of $k = 10^6\ s^{-1}$ is applied to fast unimolecular radical reactions for which no data are available. Modifications based on experimental observations concern, in particular, the shift in a hydrogen atom from the aromatic ring to an aldehyde function as proposed by Kautzman et al. (2010) or the possibility of forming a new ring with an ester function, which are described in the following sections.

The proposed chemical scheme for the oxidation of naphthalene includes 383 species (231 stable and 152 radicals) and 803 reactions (including 319 product-free sink reactions to avoid compound accumulation). The list of species includes 27 of the 29 MWs observed during the experiments of Kautzman et al. (2010). Due to the large number of secondary species involved in the progressive oxidation of naphthalene (noted as NAPH in the scheme), a specific nomenclature is applied to identify them (see Table 1).

Table 1. Species name nomenclature.

Main structure	
Na	Compound with two carbon rings (not only aromatics)
Ph	Compound with only one ring (aromatic)
Functional groups	
O	-OH gp.
K	=O gp. (ketone)
D	=O gp. (aldehyde)
H	-OOH gp.
N	-ONO_2 gp.
V	-NO_2 gp.
A	-CO(OH) gp. (acid)
G	-CO(OOH) gp.
P	-$CO(OONO_2)$ gp. (PAN)
Bp	Peroxy bridge on ring
Epox	Epoxide
Anhy	Anhydre
Est	Esther
Geometrical suffixes	
par	*para-* isomer
ort	*ortho-* isomer
Radical prefixes	
1	Carboxy radical
2	Peroxy radical
3	Acetyl peroxy radical
4	Carbon-centered radical
5-Crg	Criegee bi radical
Group position	
X-Na/Ph	X function on the non-reactive ring
Na/Ph-X	X function on the reactive ring or on an aliphatic part of the species
Other	
NaOPEN	First product after ring opening
NaOPENOL	

3 Mechanism description

3.1 Oxidation of naphthalene by OH

Scheme 1 shows the reaction of naphthalene with OH to form nitronaphthalene (NaV), naphthenol (NaO) or one of the three possible RO_2 radicals (4NaOBp, 2NaOort and 2NaOpar) depending on the OH and O_2 attack location on the aromatic ring. The kinetics rate of the NAPH + OH reaction is set at $k_{NAPH+OH} = 1.105 \times 10^{-12} \times \exp(902/T)\ s^{-1}\ molec^{-1}\ cm^3$, adapted from the studies of Shiroudi et al. (2014) and Roueintan et al. (2014) and in agreement with the experimental study of Atkinson et al. (1984).

Here, 90 % of OH addition takes place on the carbon atom in position 1 (see Scheme 1) and 10 % in position 2 (Shiroudi et al., 2014). In the scheme, no distinction is made between these two isomers (called 4NaO); however, the following branching ratios for RO_2 formation take both possibilities into account. The carbon-centered radical 4NaO can react with either NO_2 with a kinetic rate of $k_{4NaO+NO2} = 3.6 \times 10^{-11}\ s^{-1}\ molec^{-1}\ cm^3$ (Nishino et al., 2008) or O_2 with a kinetic rate of $k_{4NaO+O2} = 4.47 \times 10^{-16}\ s^{-1}\ molec^{-1}\ cm^3$ (adapted from the SAR estimations by Jenkin et al., 2018b, considering the two positional isomers and that the second aromatic ring interferes in a similar way to two alkyl groups). Following these kinetic rates, the two pathways are equivalent ($v_{4NaO+NO2} = v_{4NaO+O2}$); i.e., they have similar speeds when $[NO_2] \approx 260$ ppbv. This condition may rarely occur, perhaps only in streets with very high traffic emissions and under particular meteorological conditions. At lower NO_2 concentrations, the O_2 pathway prevails.

The branching ratios of the 4NaO + O_2 reaction, mainly related to the -OH group position and the attack position of O_2, are estimated from the SARs of Jenkin et al. (2018b, 2019), considering that the two carbons common to both rings cannot be attacked. Here, 25.5 % of the 4NaO + O_2 reactions lead to the abstraction of a hydrogen by O_2 forming the stable species NaO (considering both positional isomers of 4NaO). For molecules with the -OH group in position 1, O_2 addition essentially takes place in position 2 (*ortho-*) and then in position 4 (*para-*), enabling a double bond to be kept on the ring (impossible in position 3, *meta-*, which is therefore not considered). In relation to the 90 % of the positional isomer, the branching ratios are 54.6 % for 2NaOort and 12 % for 2NaOpar. For molecules with the -OH group in position 2, O_2 must be added in position 1 to keep a double bond, with a branching ratio of 7.9 %. The presence of the -OH group between the -OO• group and the double

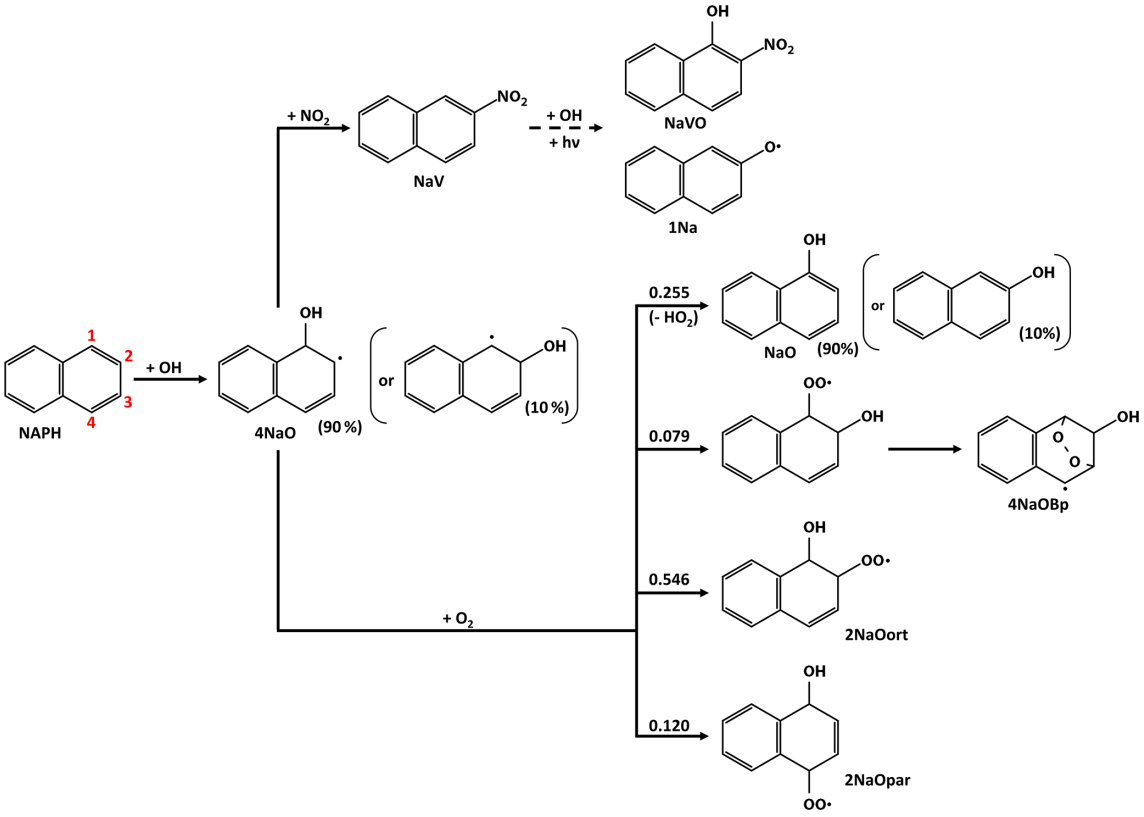

Scheme 1. First oxidation step of gaseous naphthalene by the OH radical.

bond lowers the energy barrier of the autoxidation reaction and leads to the formation of a new radical with a peroxy bridge. This reaction, impossible for 2NaOort and 2NaOpar due to molecular geometry (according to the benzene studies of Olivella et al., 2009, and Glowacki et al., 2009), is very fast in this configuration (Jenkin et al., 2019), and the formation of 4NaOBp is considered immediate. The $RO_2 + NO$ reaction may only compete with this autoxidation reaction when [NO] > 400 ppbv.

Due to the small amount of material involved in the $4NaO + NO_2$ reaction pathway, the chemistry of nitronaphthalene (NaV) is simplified in the scheme. NaV can photolyze to form an RO radical (Nojima and Kanno, 1977, adapted from benzene). The photolysis constant is adapted from the work of Phousongphouang and Arey (2003b) on monoaromatic compounds, considering the two positional isomers. The NaV reaction with OH forms 22 % nitronaphthalenol. The kinetics are roughly estimated to be 6 times slower than those of the NAPH + OH reaction by analogy with the limiting effect of NO_2-group addition on the monoaromatic compound kinetics. Products other than nitronaphthalenol are not represented.

Previous laboratory studies have shown that the NO_3-naphthalene adduct formed by the addition reaction of NO_3 on naphthalene is not stable toward the decomposition, reforming the parent (Atkinson, 1991; Atkinson and Arey, 2007; Phousongphouang and Arey, 2003a). Under atmospheric conditions, the consumption of naphthalene by its reaction with NO_3 remains negligible in most cases, compared to that with OH. This reaction is therefore not represented here.

3.2 Evolution of *para*- RO_2

Scheme 2a shows the first reaction steps of RO_2 in the *para*-position relative to the -OH group (2NaOpar). Because of its geometry, 2NaOpar cannot self-oxidize and must react with another compound: NO, NO_2, HO_2 or another RO_2 (here only CH_3O_2). This reaction leads to the formation of either (i) a stable species with a new hydroxyl, hydroperoxyl, nitrate or ketone group or (ii) the alkoxy radical 1NaOpar via oxygen abstraction, followed by NaOKpar via hydrogen abstraction by O_2 (Atkinson, 2007). Oxidation by a new OH of this compound forms 1,4-naphthoquinone (NaQuin) by abstraction of a hydrogen or a new RO_2 (2NaOOK) by O_2 addition (only one isomer is considered here). This reaction is the only pathway for naphthoquinone formation in the chemical scheme. The alkoxy radical 1NaOOK, formed after the removal of an oxygen from 2NaOOK, decomposes, leading to ring opening in positions 1–2 at 43 % or 2–3 at 57 % (see positions in Scheme 1). The chemical oxidation

scheme for the two compounds formed (PhODKD and PhDKOD) is shown in Scheme 2b. Both react in a similar way, by either photolyzing (not shown in Scheme 2b) or having a hydrogen abstracted by OH. Three sites are possible for the abstraction: the two aldehyde functions with equal probability (41 % + 41 %), forming carbonyl radicals, and the carbon linked to the alcohol group (18 %), leading to the replacement of the alcohol function by a ketone function. The latter compounds (PhKDKD and PhDKKD) will either photolyze or undergo a new H-abstraction by OH on one of their aldehyde functions. Note that in the case of a carbonyl radical directly linked to a carbon with a ketone function, the elimination of a CO and the formation of a new carbonyl radical with one fewer carbon atom is automatically considered.

All these new carbonyl radicals will follow oxidation pathways that can lead to the formation of a new ring. The key point of the proposed chemical oxidation scheme, the ring-closure scheme, is described separately in Sect. 3.6.

3.3 Evolution of *ortho*- RO_2

Scheme 3 shows the first reaction steps of RO_2 in the *ortho*-position relative to the -OH group (2NaOrt), the main pathway for the oxidation of naphthalene with OH (54.6 %). For this compound, Kautzman et al. (2010) suggest an autoxidation pathway involving the abstraction of the hydrogen from the alcohol group by the -OO• group, leading to the direct formation of one 2-formylcinnamaldehyde (NaOPEN) and an OH. The kinetic rate of this reaction is adapted here from the SAR of Jenkin et al. (2019). The 2NaOort can also react with another compound (NO, NO_2, HO_2 or CH_3O_2) to form a stable compound or an alkoxy radical (1NaOort). The 1NaOort decomposes, leading to ring opening or the formation of a new radical with an epoxide function. The evolution of 1NaOort remains highly uncertain. A theoretical study showed the tendency for the predominance of radical epoxide formation (2NaOEpox after O_2 addition) ahead of NaOPEN (Zhang et al., 2012). However, in view of the uncertainties associated with the theoretical calculation method in this previous study and our estimate of an NaOPEN formation kinetic rate higher than in the said study, it was decided to retain both reaction pathways with equal branching ratios. Furthermore, this 2NaOEpox chemistry is the only pathway for the formation of 2,3-epoxy-1,4-naphthoquinone (NaKKEpox), a major compound observed in experiments (Chan et al., 2009; Edwards et al., 2022; Kautzman et al., 2010).

NaOPEN is a major product of naphthalene oxidation (Kautzman et al., 2010). In the proposed chemical scheme, NaOPEN can react with OH or photolyze. OH is added to one of the two unsaturated carbons to form a new RO_2 by addition of O_2 (52 %; the positional isomers are grouped together as 2PhDOD) or it abstracts the hydrogen from one of the two aldehyde groups (28 % + 20 %). The two carbonyl radicals then evolve according to the ring-closure scheme (see Sect. 3.6). The 2PhDOD reacts with NO, NO_3, HO_2, OH or CH_3O_2 to form the alkoxy radical 1PhDOD, which decomposes into glyoxal and phthaldialdehyde (PhDD; see Scheme 4), another major product of naphthalene oxidation (Edwards et al., 2022; Kautzman et al., 2010).

3.4 Evolution of the radical product of naphthalene with a peroxy bridge

Scheme 4 shows the first reaction steps of the carbon-centered radical with a peroxy bridge (4NaOBp). The 4NaOBp evolves by (i) breaking the peroxy bridge to form an epoxide group and an alkoxy radical group (1NaEpox; 25 %) or (ii) adding O_2 and thus forming a new RO_2 (2NaOBp; 75 %). The branching ratio is taken to be similar to that of benzene in MCM and GECKO-A. The 1NaOEpox decomposes, leading to ring opening and to the formation of two aldehyde groups. Similarly to NaOPEN, oxidation by OH leads to the abstraction of a hydrogen from one of the aldehyde groups (same probability in this case) and chemistry continues according to the ring-closure scheme (see Sect. 3.6). The 2NaOBp reacts with NO, NO_3, HO_2 or CH_3O_2 to form a stable species or the alkoxy radical 1NaOBp, whose peroxy bridge is broken, leading to the opening of the carbon ring and the formation of the alkoxy radical with two aldehyde functions, 1PhDOD. As mentioned in Sect. 3.3, 1PhDOD decomposes into PhDD and glyoxal. The PhDD either photolyzes or sees the hydrogen of one of its aldehyde groups abstracted by OH. Its evolution then follows the ring-closure scheme (Sect. 3.6).

3.5 Hydroxynaphthalene and dihydroxynaphthalene chemistry

Scheme 5 shows the oxidation pathways of hydroxynaphthalene (NaO) according to our chemical scheme. Bunce et al. (1997) experimentally estimated $k_{NaO+OH} \approx 5 \times 10^{-10}\,s^{-1}\,molec^{-1}\,cm^3$, but to the best of our knowledge, there is no study providing detailed and combined mechanistic and kinetic data for NaO oxidation. We therefore consider here that the presence of the -OH group on one ring increases its reactivity by a factor of 10 without modifying that of the other ring. This leads to a kinetic rate with OH 5 times higher for NaO than NAPH ($k_{NaO+OH} = 1.35 \times 10^{-10}\,s^{-1}\,molec^{-1}\,cm^3$) on the same order of magnitude as the Bunce et al. (1997) estimation. For comparison, according to MCM kinetic data, the addition of an -OH function to benzene or toluene or to o-, m-, or p-xylenes results in an increase in oxidation kinetic rates by a factor of 23, 8.6, 5.9, 3.5 or 5.7 at 298 K, respectively. The functionalized aromatic ring is later called the "reactive" ring, as the non-functionalized one is later called the "non-reactive" ring. In the absence of data, it is assumed that hydrogen abstraction from the alcohol group accounts for 6 % of the total, equal to that of phenol in MCM. The other branching ratios of the NaO + OH reaction take into account the 10-times-

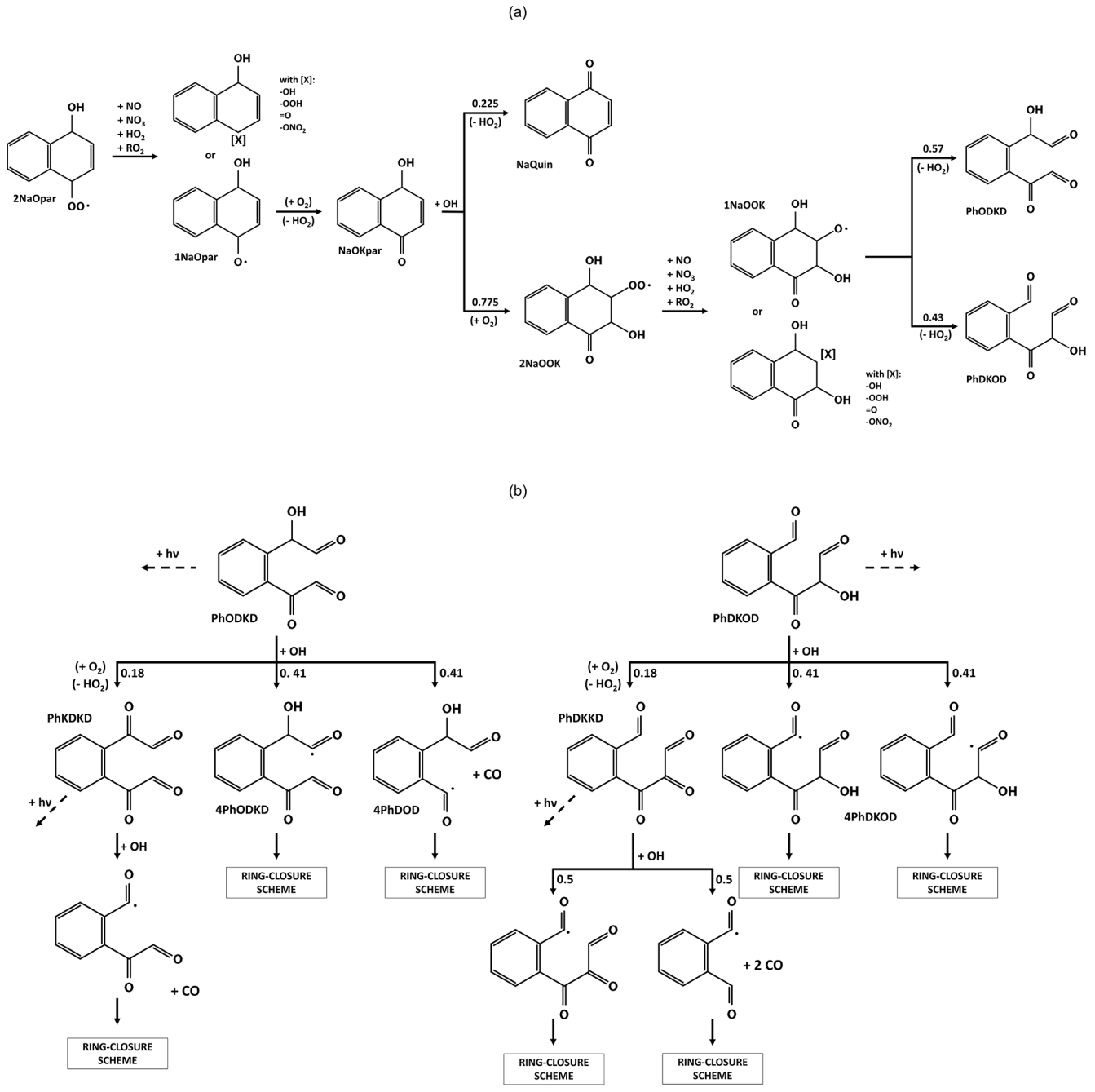

Scheme 2. Evolution of naphthalene secondary compounds after the addition of O_2 in the *para*- position of the OH group **(a)** until and **(b)** after ring opening.

greater reactivity of the reactive ring and the ∼ 25 % : 75 % ratio between the addition of a new -OH function and the formation of a new RO_2 from the NAPH + OH reaction. Thus, the reaction leads to (i) the formation of dihydroxynaphthalene with the addition of the new function on the reactive ring (NaOO) at 21.4 % or on the non-reactive one (ONaO) at 2.1 % or (ii) the formation of RO_2 by the successive addition of OH and O_2 at 64.1 % on the reactive ring or 6.4 % on the non-reactive one.

The alkoxy radical 1Na reacts with O_3, NO_2 or HO_2, forming the associated RO_2 2Na or NaVO or reforming NaO, respectively. As mentioned in Sect. 2, the kinetic rates of these reactions are adapted from Tao and Li (1999), Platz et al. (1998), and Mousavipour and Homayoon (2011). The 2Na

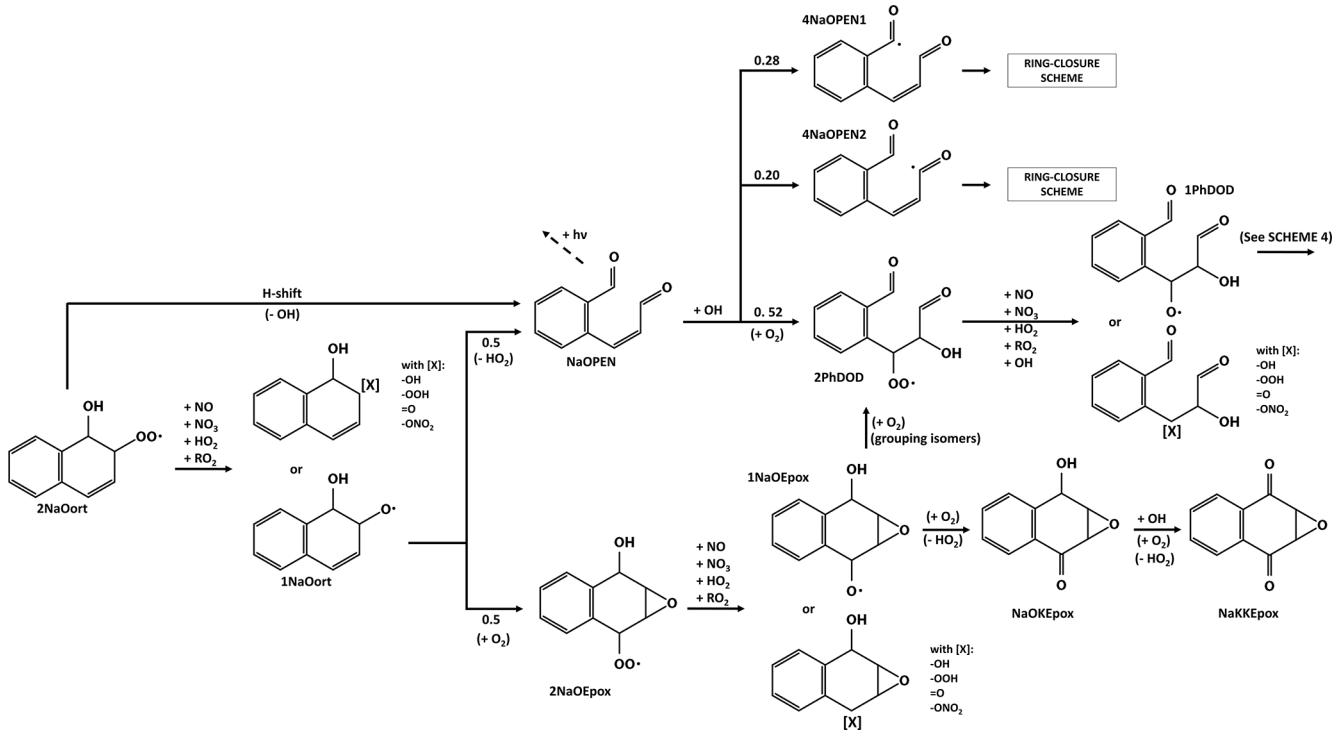

Scheme 3. Evolution of naphthalene secondary compounds after the addition of O_2 in the *ortho-* position of the OH group.

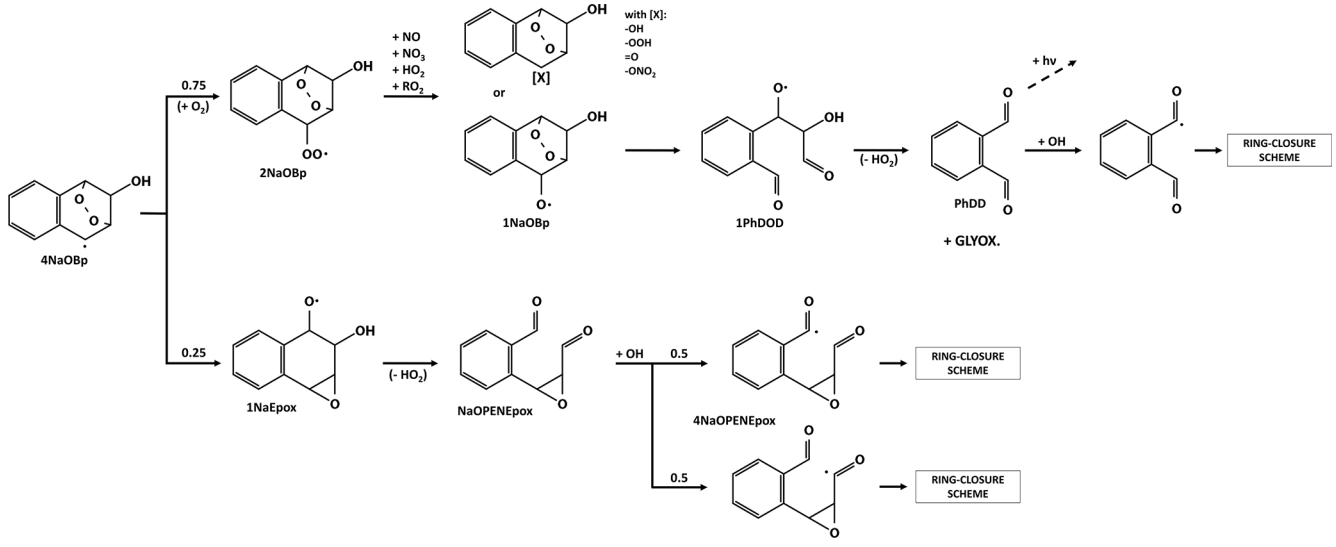

Scheme 4. Evolution of naphthalene secondary compounds after the formation of a peroxy bridge.

then reacts with NO, NO_2, NO_3, HO_2 or CH_3O_2 to form NaO or the hydroperoxynaphthalene NaH.

For the RO_2 formation pathway with OH addition on the non-reactive ring (2ONaO), the branching ratios between the various positional isomers are similar to those of the NAPH reaction considering (i) the 90 % : 10 % ratio for OH addition in positions 1 and 2, respectively (see Scheme 1 for positions); (ii) the O_2 addition in *ortho-* at 82% (2ONaOort) or in *para-* at 18 % (2ONaOpar) when the -OH group is in position 1; and (iii) the immediate formation of a peroxy bridge (4ONaOBp) when the -OH group is in position 2. For the RO_2 formation pathway with OH addition on the reactive ring (2NaOO), branching ratios for the different OH addition positions (related to the first -OH group) are adapted from Jenkin et al. (2018b): 50 % in the *ortho-* position and 50 % in the *para-* position. For a molecule with both -OH

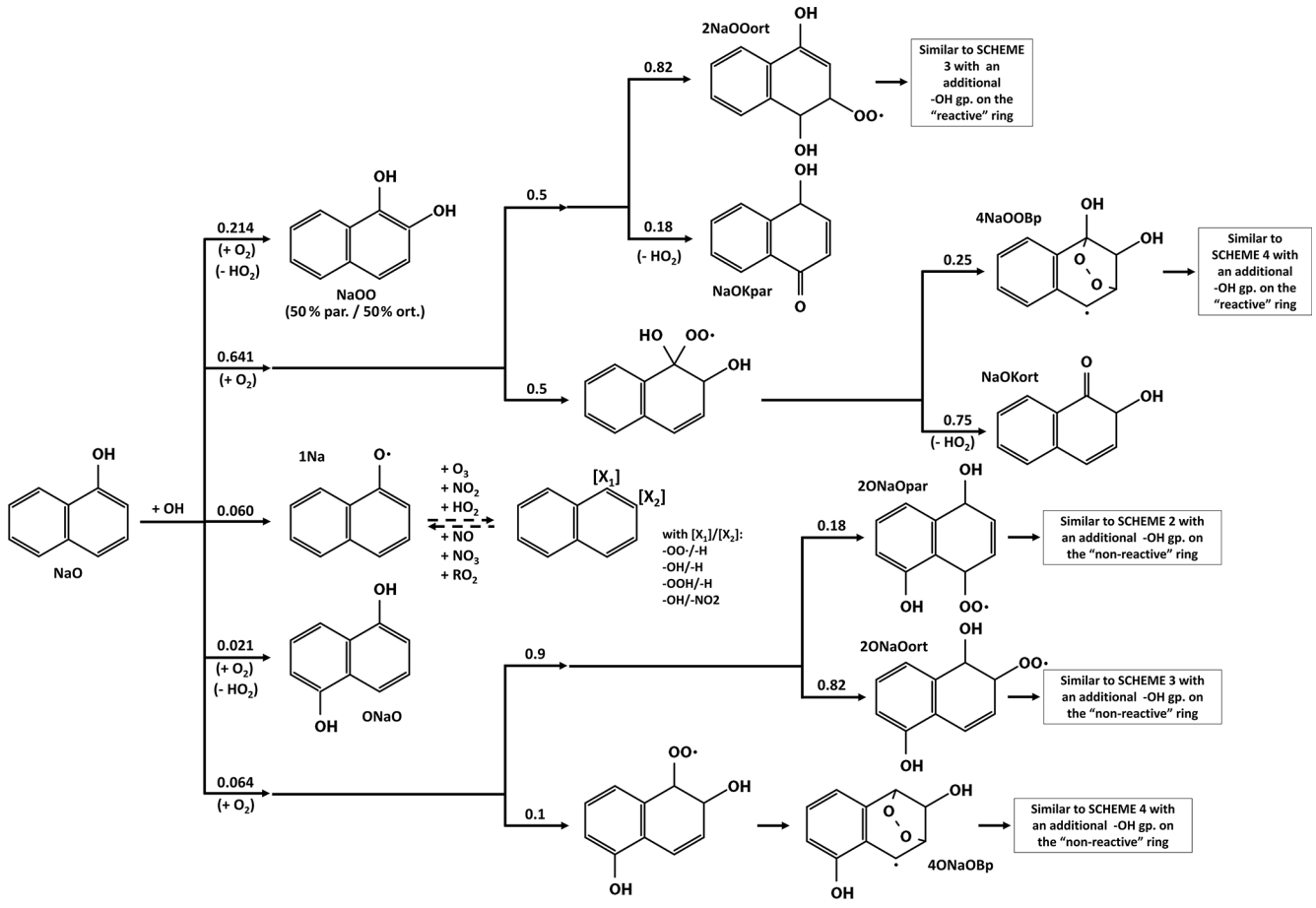

Scheme 5. Oxidation of gaseous hydroxynaphthalene by the OH radical.

groups in *para*- position, an O_2 is added to a free carbon at 82 % (2NaOOort) and to a carbon bearing an -OH function at 18 %, leading to the formation of a ketone function by HO_2 elimination (NaOKpar). For a molecule with two -OH groups in *ortho*- position, an O_2 is added to a carbon with an -OH function. Ketone formation by hydrogen abstraction becomes competitive with peroxy bridge formation (Jenkin et al., 2019). In the absence of precise kinetic data, a ratio of 25 % : 75 % is applied for the peroxy bridge (4NaOOBp) and ketone (NaOKort) formation pathways. The 2NaOOort, 4NaOOBp, 2ONaOpar, 2ONaOort and 4ONaOBp then evolve following Schemes 2, 3 or 4, considering the presence of an additional OH function.

Scheme 6 shows the oxidation pathways of dihydroxynaphthalene (NaOO) according to our chemical scheme. Similar to NaO, no precise mechanistic and kinetic data are available for the oxidation of NaOO. We consider that the addition of the second -OH function increases the kinetic rate of the reactive ring by a factor of 3.5 compared to the NaO one (average increases between hydroxy and dihydroxy aromatic compound kinetic rates for benzene, toluene and o-xylene in the MCM), without altering the kinetic rate of the non-reactive ring. This leads to a reaction kinetic rate of $k_{\mathrm{NaOO+OH}} = 4.96 \times 10^{-10}\,\mathrm{s^{-1}\,molec^{-1}\,cm^3}$.

According to kinetics and branching ratios, only 5 % of the NAPH potentially evolves into NaOO. The NaOO chemical diagram is therefore simplified by not considering oxidation on the non-reactive ring and by grouping together some of the isomers formed. The reaction leads to (i) the abstraction of hydrogen from one of the -OH functions (1NaO; 6 %), (ii) the addition of a third -OH function on the reactive ring (NaOOO; 23 %), or (iii) the successive addition of OH and O_2 forming a new RO_2 on the reactive ring (2NaOOO; 71 %).

The chemistry of 1NaO is similar to that of 1Na. Branching ratios for 2NaOOO evolution take into account the two positional isomers of NaOO (50 % *ortho*- and 50% *para*-) and the competitiveness of the ketone-forming pathway with regard to peroxy bridge formation when O_2 adds on to a carbon with an -OH function (a 50 % : 50 % ratio is considered here). The 2NaOOOBp groups together different positional isomers. The kinetics data of the 2NaOOOBp reaction with NO, HO_2, NO_3 and CH_3O_2, as well as its decomposition and ketone formation, are estimated with the SAR of Jenkin et al. (2019). This chemistry leads in part to the open-

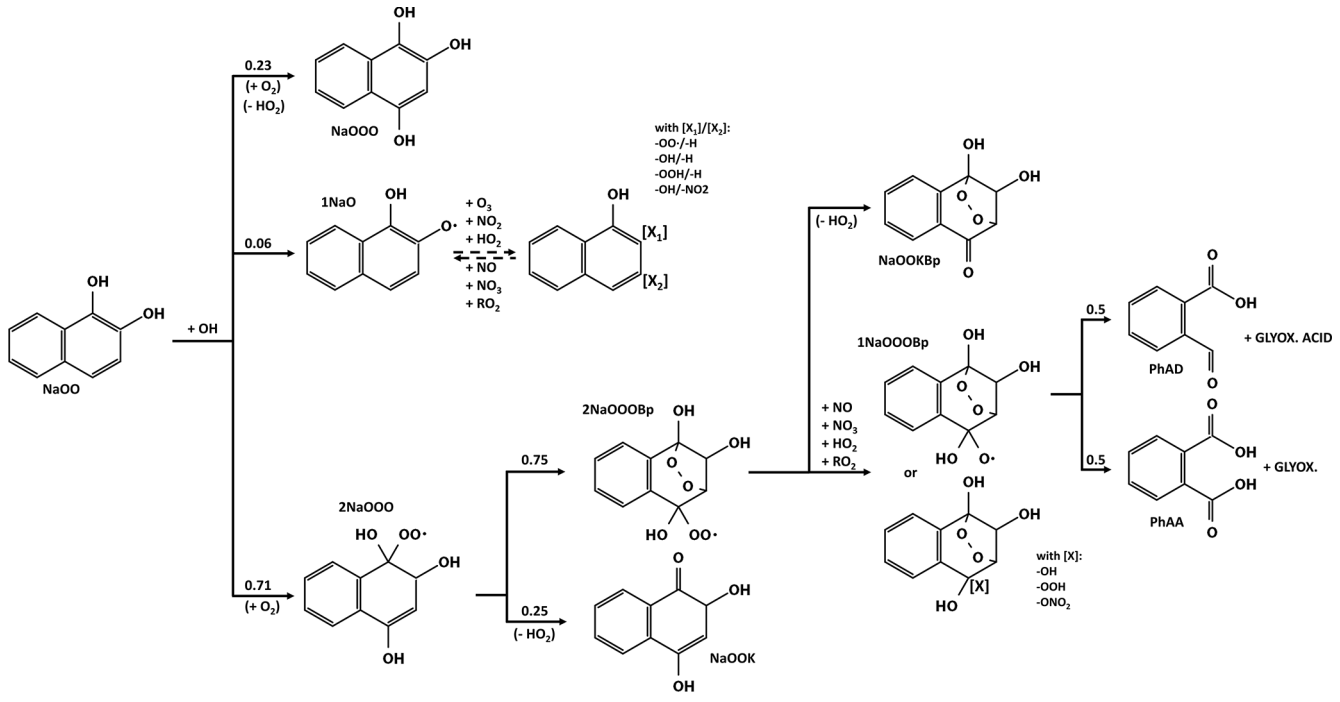

Scheme 6. Oxidation of gaseous dihydroxy naphthalene by the OH radical.

ing of the reactive ring and the formation of phthalic acid (PhAA), phthalaldehydic acid (PhAD), glyoxal and glyoxalic acid, which have been observed in naphthalene oxidation experiments (Kautzman et al., 2010).

3.6 Ring closure and opened ring chemistry

A key element of the new chemical scheme is the possibility, after the opening of an aromatic ring, of forming a new ring with an ester or anhydride function. The generic chemical scheme for this process is shown in Scheme 7. Ring closure is considered possible in three scenarios: the removal of hydrogen from one of the two aldehyde functions of a dialdehyde, followed by the addition of the oxygen from the second function to form a new radical (case 1); the intra-molecular attack of an aldehyde function by a radical oxygen of an acyloxy function, with the removal of a hydrogen by an O_2 molecule (and the formation of HO_2; case 2); or the intra-molecular attack of an acid function by a radical oxygen of an acyloxy function, with the release of an OH radical (case 3). This ring-closure process competes with the addition of an O_2 in case 1 and with the formation of a carbonyl radical by the loss of a CO_2 molecule in cases 2 and 3. With no kinetic data available, a branching ratio of 60 % : 40 % in favor of ring closure is applied for cases 2 and 3, similar to that proposed by Bloss et al. (2005) for the formation of maleic anhydride. An inverse ratio of 40 % : 60 %, unfavorable to ring closure, is applied to case 1, similar to that proposed by Bloss et al. (2005) for the photolysis of butenedial and formation of the corresponding furanone (photolysis leading to hydrogen abstraction from one of butenedial's aldehyde functions). The kinetic and mechanistic data of the intermediate steps are estimated using GECKO-A SARs.

The ring-closure pathway, proposed in a simplified way without kinetic and mechanistic data by Kautzman et al. (2010) for phthaldialdehyde (PhDD), is here detailed, completed and applied to all aromatic dialdehydes in the chemical scheme (from C8 to C10). However, to limit the complexity of the scheme, this chemistry is represented according to three levels of precision: (i) application of the ring-closure scheme to both carbonyl radicals (depending on the position of the hydrogen abstraction) for pathways involving more than 5 % of the initial molecules, (ii) grouping of the two carbonyl radicals into one and application of the ring-closure scheme for pathways involving between 1 % and 5 % of the initial molecules, and (iii) direct formation of the final products for pathways involving less than 1 % of the initial molecules.

Gaseous reactions between the anhydrides and H_2O are included in the chemical scheme. In the absence of data, the kinetics of these reactions are considered equal to those of N_2O_5 with H_2O: $k_{ahhy+H2O} = 2.5 \times 10^{-22}$ s^{-1} molec^{-1} cm^3. The fragmentation of molecules and loss of CO_2 represented in the ring-closure scheme (Scheme 7) can lead to the formation of radicals with a free electron on the aromatic ring (see Scheme 8). When such a radical is formed and has an aliphatic chain of at least 2 carbon atoms ending in an aldehyde function, an H-shift occurs, as shown in Scheme 8. This mechanism was initially proposed by Kautzman et al. (2010)

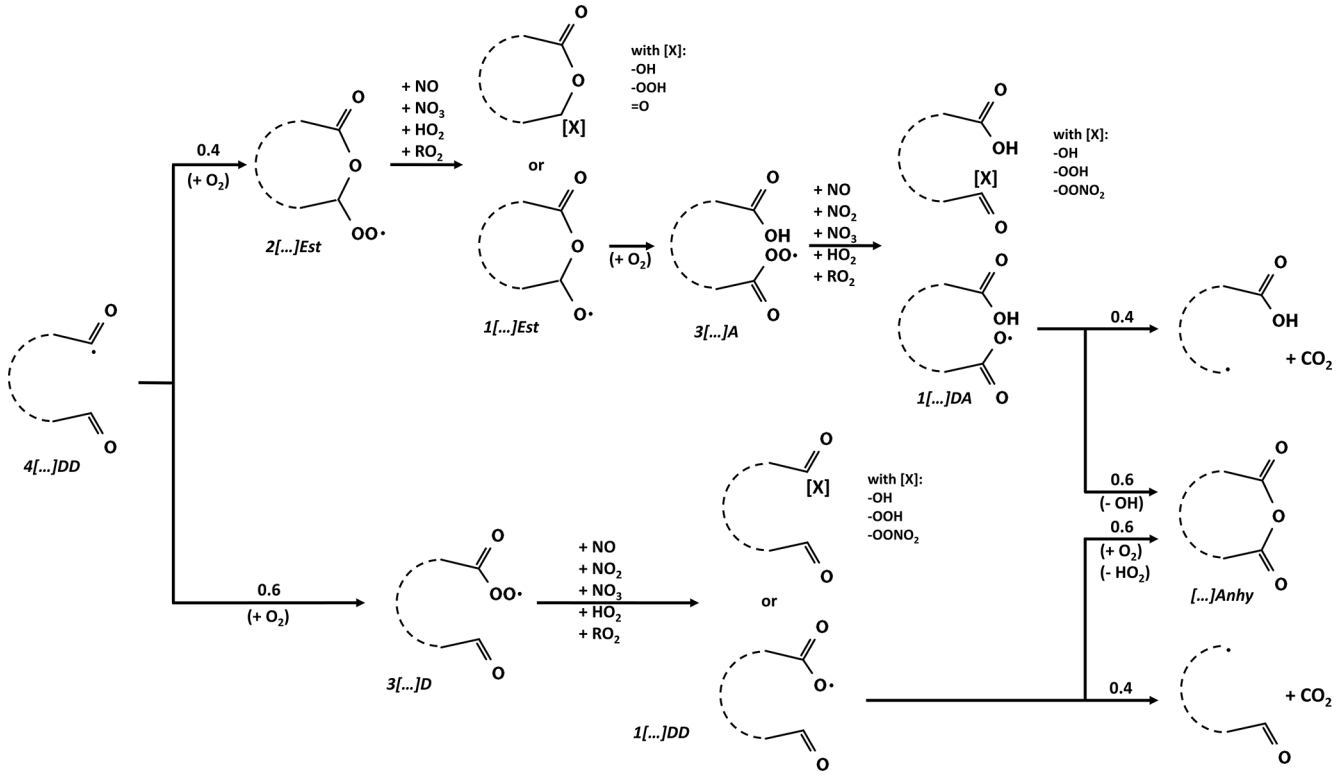

Scheme 7. Ring-closure scheme – Oxidation scheme of gaseous dialdehydes leading to the formation of an ester or anhydrous new ring. Generic annotations for molecule names are shown in italics.

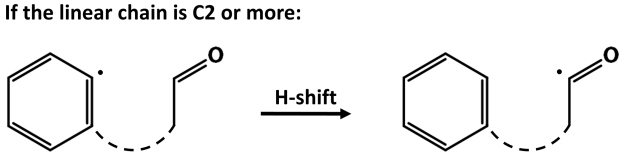

Scheme 8. H-shift from aldehyde carbon to the aromatic one proposed by Kautzman et al. (2010). Only considered here when the linear chain includes two or more carbon atoms (de facto excluding the benzaldehyde radical).

as a possible route for the formation of C7 and C9 compounds.

3.7 Other represented reactions

In our scheme, the chemistry leading to the opening of the second aromatic ring is not represented, as the compounds involved have not been observed in significant quantities in naphthalene oxidation experiments (Chan et al., 2009; Edwards et al., 2022; Kautzman et al., 2010). Glyoxal and C1 chemistry are considered. Finally, to avoid compound accumulation, product-free loss reactions are added for all compounds whose chemistry is not represented. In the case of PAN loss reactions, thermal decomposition reactions releasing NO_2 still have products (NO_2+ acyl peroxy radical).

4 Naphthalene oxidation modeling

4.1 Simulation parameters

Test simulations of the naphthalene chemical scheme have been carried out using the SSH-aerosol model (Sartelet et al., 2020). These tests reproduce the oxidation of naphthalene in an oxidation flow reactor (OFR) under experimental conditions similar to those presented in Lannuque et al. (2023) for toluene. Briefly, as described in Martinez (2019), 140 ppbv of isopropyl nitrite (IPN), 17 ppbv of naphthalene and 200 ppbv of NO_2 are introduced into an OFR irradiated with UV lamps. Temperature is set at 280 K and relative humidity at 37 %. Then, 9.3 µg m^{-3} of ammonium sulfate is introduced as seed for condensation. Photolysis of IPN generates additional NO_x and OH radicals for oxidation. Residence time in the OFR is around 13 min. An SOA concentration of 6.6 µg m^{-3} is experimentally measured at the OFR outlet by a high-resolution time-of-flight aerosol mass spectrometer (HR-ToF-AMS, Tofwerk AG, Aerodyne Inc., USA; Martinez, 2019). Instrumentation and measurement techniques are detailed in Lannuque et al. (2023).

In the simulation, inorganic chemistry is represented as in the regional atmospheric chemistry mechanism, version 2 (RACM2) scheme (Goliff et al., 2013), IPN photolysis is represented as described in Lannuque et al. (2021) and a wall loss parameterization of gaseous compounds as presented in

Lannuque et al. (2023) is applied. Gas–particle partitioning is represented dynamically, considering transfers toward both the organic and aqueous phases of the aerosol. Interactions between molecules within condensed phases are represented using the Universal Quasi-chemical Functional-group Activity Coefficients (UNIFAC; Fredenslund et al., 1975) and the Aerosol Inorganic–Organic Mixtures Functional groups Activity Coefficients (AIOMFAC; Zuend et al., 2008) methods. Saturation vapor pressures (P^{sat}) of stable compounds are (i) derived from the measured experimental value of naphthalene for the PAHs or (ii) estimated using the SAR from Nannoolal et al. (2008, 2004) for the others. Henry's law constants are calculated from the UNIFAC groups of the compounds and their P^{sat}. The simulation time is fixed equal to the residence time in the OFR: 13 min. Simulated speciation is here qualitatively compared to the experimental observations of Kautzman et al. (2010) and Edwards et al. (2022).

4.2 Simulation results

The final simulated concentrations of each species in both gaseous and condensed phases are detailed in the Supplement. Naphthalene oxidation with the new chemical scheme leads to the formation of 6.0 µg m^{-3} of SOA, close to but 9 % lower than the measured concentration (6.6 µg m^{-3}). Figure 1 shows the chemical characteristics of simulated naphthalene reaction products at 280 K in both the gaseous and particulate phases.

The mass distribution of gaseous secondary organic compounds is dominated by C8 (39 %) and C10 (39 %). The C2 fraction, almost exclusively composed of glyoxal, is the third largest at 17 %, ahead of C7 (3 %) and C9 (1 %). The C1, C3, C4, C5 and C6 fractions are negligible. Overall, gaseous secondary compounds are little oxidized, with only 25 % containing four or more oxygen atoms (18 % with five or more atoms). The most oxidized compounds (four oxygens or more) are mainly C8 (12 %), C10 (10 %) and C7 (3 %). The mass distribution of secondary organic compounds in the condensed phase is overwhelmingly dominated by C10 (78 %), followed by C8 (13 %), C7 (7 %) and C9 (2 %). No simulated compounds with fewer than seven carbon atoms are found in the condensed phase. Condensed compounds are highly oxidized overall, with about 90 % having four or more oxygen atoms and 50 % having six or more. The simulated molar mass distribution shows that the gaseous secondary compounds are evenly distributed between heavy compounds, with 52 % of the total mass having MW $\geq$ 150 g mol^{-1}, and lighter ones, with 48 % having MW $<$ 150 g mol^{-1} (for comparison, the MW of naphthalene is 128 g mol^{-1}). Note that the 17.4 % with MW $<$ 100 g mol^{-1} is almost exclusively glyoxal. In the condensed phase, the distribution shows a broad predominance of heavy compounds, with 98 % of the mass having MW $\geq$ 150 g mol^{-1} and 64 % MW $\geq$ 200 g mol^{-1}.

The predominance of C10 and C8 among naphthalene oxidation products is in agreement with experimental observations at high NO_x (Edwards et al., 2022; Kautzman et al., 2010). However, the model seems to underestimate the formation of C9, also measured (in smaller quantities than C10 and C8) in these studies. It also appears that the model preferentially forms heavy compounds (MW $\geq$ 200 g mol^{-1}) that are not observed in experiments. The heaviest compound observed in significant concentrations has a MW of 208 g mol^{-1} (Edwards et al., 2022; Kautzman et al., 2010).

Figure 2 shows the reconstruction of the mass spectrum (in MW) with simulated concentrations. In the gas phase, five major peaks stand out: glyoxal at MW = 58 g mol^{-1} (7.3 µg m^{-3}); phthalaldehyde PhDD at MW = 134 g mol^{-1} (10 µg m^{-3}); the peak at MW = 160 g mol^{-1} corresponding to NaOPEN, NaOKpar, NaOKort, and NaOO (5.2 µg m^{-3} in total); the nitronaphthalene peak of NaV at MW = 173 g mol^{-1} (2.9 µg m^{-3}); and that of PAN PhPD at MW = 211 g mol^{-1} (3.9 µg m^{-3}). For the particulate phase, the main peaks are at MW $>$ 174 g mol^{-1}. The main ones are the PhDKOD and PhODKD isomers at MW = 192 g mol^{-1} (1.1 µg m^{-3} in total), the OPhODKD peak at MW = 208 g mol^{-1} (0.6 µg m^{-3}), the PAN PhPA peak at MW = 227 g mol^{-1} (0.7 µg m^{-3}), and the one at MW = 239 g mol^{-1} corresponding to PhDNOD and NaNOOK (1.5 µg m^{-3} in total).

The model represents a large fraction of the MW associated with the major experimental compounds well (58, 134 or 192 g mol^{-1}, for example) but underestimated some others (148, 150, 162 or 166 g mol^{-1}, for example; Edwards et al., 2022; Kautzman et al., 2010). There are two main reasons for these underestimations. Firstly, for the anhydrides (such as PhAnhy at MW = 149 g mol^{-1}), the model misrepresents the hydration reactions of anhydrides that are not represented in the aqueous phase and whose kinetics are based on N_2O_5 in the gas phase. Furthermore, temperatures reached during measurement (between 60 and 130 °C according to Martinez, 2019) can lead to the formation of additional anhydrides, fueling the discrepancies observed for these compounds. Secondly, mass spectrometry methods tend to fragment compounds with a nitrate or PAN function, resulting in the loss of NO_2 (Müller et al., 2012). This may explain the absence of such compounds among the major observed ones, even under high-NO_x conditions (Edwards et al., 2022; Kautzman et al., 2010). It appears that the majority of compounds formed with MW $\geq$ 200 g mol^{-1} according to the model are compounds with at least one nitrate or PAN function (yellow bars in Fig. 2). This could explain the simulated peak at MW = 207 g mol^{-1}, which actually corresponds to the measurement at MW = 162 g mol^{-1} that was identified as a majority compound in the study of Edwards et al. (2022).

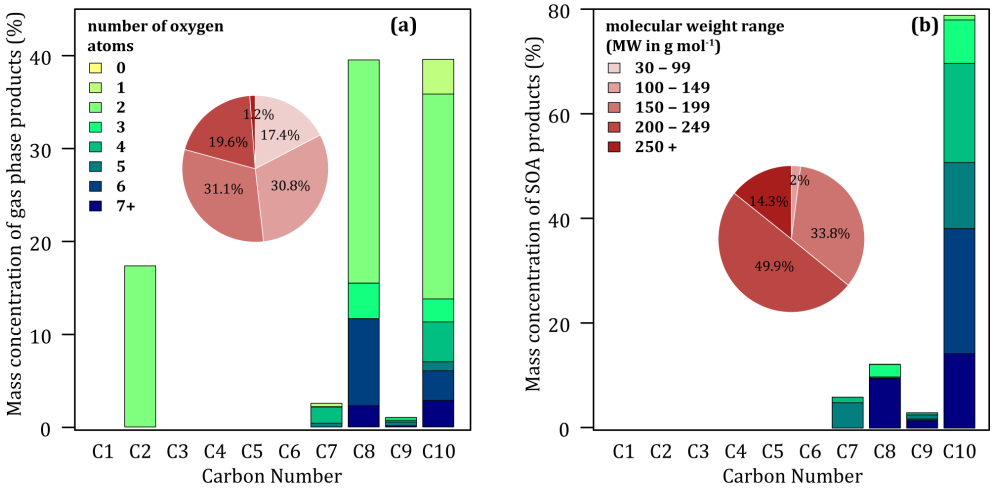

Figure 1. Simulated mass product fraction (y axis) distribution based on the number of carbon atoms (x axis) for the oxidation of 17 ppbv naphthalene at 37 % RH and 280 K in the gas **(a)** and the condensed **(b)** phases. Pie charts show the molecular weight contribution to the overall mass.

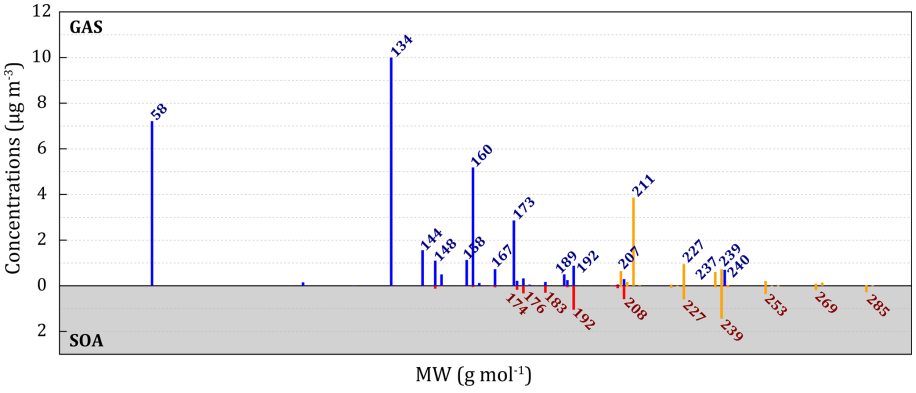

Figure 2. Mass spectra (m/z) of gaseous (blue) and condensed (red) secondary compounds for the simulated oxidation of 17 ppbv naphthalene at 280 K. The yellow fractions of the spectra represent compounds with nitrate or PAN functions.

5 Limits and perspectives

The simulation presented has some limitations, and improvements could be made to the model. Considering the irreversible partitioning of glyoxal to the condensed phase (Hu et al., 2022), as was done for methylglyoxal produced during toluene oxidation in a previous study (Lannuque et al., 2023), could lead to an increase in the simulated SOA concentration and thus to a reduction in the difference between simulated and observed OA. In terms of speciation, the chemical scheme detailed in this article, while sufficient to reproduce the experimental major products, only represents the first stages of naphthalene oxidation by OH. The reaction of naphthalene with NO_3, although kinetically slower than that with OH under most environmental conditions, has been studied (Atkinson, 1991; Atkinson and Arey, 2007; Phousongphouang and Arey, 2003a) and can easily be added to the scheme if required. Many kinetics and reaction pathways are estimated using SARs or extrapolated from similar compounds. Areas for improvement are therefore conceivable. The chemical scheme does not represent the opening of the second aromatic ring. The oxidation of monoaromatic compounds, which is better studied, is already represented in the detailed chemical diagrams of MCM or GECKO-A. It is entirely feasible to couple one of these two schemes to the one presented in this article to represent the entire oxidation of naphthalene. In the absence of experimental or theoretical data, some kinetics and/or branching ratios have been set arbitrarily, similar to those of other compounds. This is the case for the gaseous reactivity of anhydrides with H_2O, whose kinetics have been fixed equal to those of N_2O_5 and deserve to be studied better and adjusted in view of the discrepancies in the concentrations of these compounds. This is also the case for branching ratios leading to the closure and formation of the new ester ring. These were taken directly from data on the formation of maleic anhydride or fu-

rans in the MCM (Bloss et al., 2005), without adaptation to the molecules in the scheme. It is conceivable that these ratios could be adjusted to match observations better or after a specific study of this type of reactivity. More generally, the choice not to consider the possibility of peroxy bridge formation straddling the two aromatic rings needs to be studied in order to be validated or not.

In the long term, given the redundancy of the reaction steps in the naphthalene scheme, we can imagine automating its generation in the same way as GECKO-A and applying different steps to the generation of schemes for different PAHs. As naphthalene is the simplest of the PAHs, there are still barriers to overcome for automatic generation of chemical schemes for more complex compounds, such as quantifying the impact on reactivity of (i) the presence of alkyl, oxygenated or halogenated groups or (ii) the increase in aromatic ring numbers and their arrangement.

6 Summary

For the first time, a detailed chemical scheme for the oxidation of naphthalene by OH with kinetic and mechanistic data is proposed. The scheme redundantly represents all the classical steps of atmospheric organic chemistry: (i) the formation of carbon-centered radicals by oxidation or photolysis of stable compounds; (ii) the addition of O_2 (forming RO_2) or NO_2; (iii) the reaction of RO_2 with NO, NO_2, NO_3, HO_2, or CH_3O_2 or its autoxidation; and (iv) the evolution of RO by decomposition, isomerization, or reaction with O_2. Kinetic and mechanistic data were estimated using SARs or by analogy with existing experimental or theoretical data. The proposed chemical scheme includes 383 species (231 stable species) and 803 reactions, representing 93 % of the major MW observed in previous experimental studies.

A first simulation reproducing experimental oxidation in OFR under high-NO_x conditions shows the reproduction of SOA mass formed on the same order of magnitude as was experimentally observed, with an error of −9 %. The simulated gaseous oxidation products of naphthalene are mainly C8 (39 %) and C10 (39 %) and oxidize slightly (less than four oxygen atoms), whereas the simulated SOA is largely dominated by more-oxidized C10 (78 %). A large fraction of the simulated SOA consists of heavy compounds (64 % with MW > 200 g mol^{-1}) with nitrate or PAN functions. The model overestimation of nitrates and PANs with high MW can be partly explained by the frequent fragmentation of these compounds during measurements. Taking this process into account improves the model representation of speciation.

The writing in redundant steps of this new detailed chemical scheme for the oxidation of naphthalene should eventually enable it to be written automatically and is a first step towards the writing of more complex chemical schemes for the oxidation of PAHs.

Code and data availability. Chemical scheme and modeling data analyzed in the article are available in the Supplement. The SSH-aerosol model is open-source (GNU GPL-3 license). SSH-aerosol version 1.3 is available at https://doi.org/10.5281/zenodo.10159225 (Sartelet et al., 2022).

Supplement. The supplement related to this article is available online at: https://doi.org/10.5194/acp-24-8589-2024-supplement.

Author contributions. VL designed the research, developed the scheme, ran the simulation and drafted the article. VL and KS revised the article and were responsible for funding acquisition.

Competing interests. The contact author has declared that neither of the authors has any competing interests.

Disclaimer. Publisher's note: Copernicus Publications remains neutral with regard to jurisdictional claims made in the text, published maps, institutional affiliations, or any other geographical representation in this paper. While Copernicus Publications makes every effort to include appropriate place names, the final responsibility lies with the authors.

Acknowledgements. The authors gratefully acknowledge Barbara D'Anna for numerous discussions about and clarifications regarding experimental and measurement methods and for advice on the processing and interpretation of experimental data.

Financial support. This work was funded by the POLEMICS project of the Agence Nationale de la Recherche (ANR) program (grant no. ANR-18-CE22-0011), DIM QI^2 (an air quality research network in the Ile-de-France region) and the MAESTRO-EU6 project (ADEME CORTEA no. 1866C0001). This work also benefited from the IPSL-CGS EUR.

Review statement. This paper was edited by Kelley Barsanti and reviewed by two anonymous referees.

References

Appel, K. W., Napelenok, S. L., Foley, K. M., Pye, H. O. T., Hogrefe, C., Luecken, D. J., Bash, J. O., Roselle, S. J., Pleim, J. E., Foroutan, H., Hutzell, W. T., Pouliot, G. A., Sarwar, G., Fahey, K. M., Gantt, B., Gilliam, R. C., Heath, N. K., Kang, D., Mathur, R., Schwede, D. B., Spero, T. L., Wong, D. C., and Young, J. O.: Description and evaluation of the Community Multiscale Air Quality (CMAQ) modeling system version 5.1, Geosci. Model Dev., 10, 1703–1732, https://doi.org/10.5194/gmd-10-1703-2017, 2017.

Arey, J., Zielinska, B., Atkinson, R., and Winer, A. M.: Polycyclic aromatic hydrocarbon and nitroarene concentrations in ambient air during a wintertime high-NOx episode in the Los Angeles basin, Atmos. Environ., 21, 1437–1444, https://doi.org/10.1016/0004-6981(67)90091-1, 1967.

Arey, J., Atkinson, R., Zielinska, B., and McElroy, P. A.: Diurnal concentrations of volatile polycyclic aromatic hydrocarbons and nitroarenes during a photochemical air pollution episode in Glendora, California, Environ. Sci. Technol., 23, 321–327, https://doi.org/10.1021/es00180a009, 1989.

Atkinson, R.: Kinetics and Mechanisms of the Gas-Phase Reactions of the NO_3 Radical with Organic Compounds, J. Phys. Chem. Ref. Data, 20, 459–507, https://doi.org/10.1063/1.555887, 1991.

Atkinson, R.: Rate constants for the atmospheric reactions of alkoxy radicals: An updated estimation method, Atmos. Environ., 41, 8468–8485, https://doi.org/10.1016/j.atmosenv.2007.07.002, 2007.

Atkinson, R. and Arey, J.: Mechanisms of the gas-phase reactions of aromatic hydrocarbons and PAHs with OH and NO_3 radicals, Polycycl. Aromat. Compd., 27, 15–40, https://doi.org/10.1080/10406630601134243, 2007.

Atkinson, R., Aschmann, S. M., and Pitts, J. N.: Kinetics of the Reactions of Naphthalene and Biphenyl with OH Radicals and with O_3 at 294 ± 1 K, Environ. Sci. Technol., 18, 110–113, https://doi.org/10.1021/es00120a012, 1984.

Atkinson, R., Aschmann, S. M., Arey, J., and Carter, W. P. L.: Formation of ring-retaining products from the OH radical-initiated reactions of benzene and toluene, Int. J. Chem. Kinet., 21, 801–827, https://doi.org/10.1002/kin.550210907, 1989.

Aumont, B., Szopa, S., and Madronich, S.: Modelling the evolution of organic carbon during its gas-phase tropospheric oxidation: development of an explicit model based on a self generating approach, Atmos. Chem. Phys., 5, 2497–2517, https://doi.org/10.5194/acp-5-2497-2005, 2005.

Baek, S. O., Field, R. A., Goldstone, M. E., Kirk, P. W., Lester, J. N., and Perry, R.: A review of atmospheric polycyclic aromatic hydrocarbons: Sources, fate and behavior, Water. Air. Soil Pollut., 60, 279–300, https://doi.org/10.1007/BF00282628, 1991.

Bloss, C., Wagner, V., Jenkin, M. E., Volkamer, R., Bloss, W. J., Lee, J. D., Heard, D. E., Wirtz, K., Martin-Reviejo, M., Rea, G., Wenger, J. C., and Pilling, M. J.: Development of a detailed chemical mechanism (MCMv3.1) for the atmospheric oxidation of aromatic hydrocarbons, Atmos. Chem. Phys., 5, 641–664, https://doi.org/10.5194/acp-5-641-2005, 2005.

Boström, C.-E., Gerde, P., Hanberg, A., Jernström, B., Johansson, C., Kyrklund, T., Rannug, A., Törnqvist, M., Victorin, K., and Westerholm, R.: Cancer risk assessment, indicators, and guidelines for polycyclic aromatic hydrocarbons in the ambient air., Environ. Health Perspect., 110, 451–488, https://doi.org/10.1289/ehp.110-1241197, 2002.

Boucher, O., Randall, D., Artaxo, P., Bretherton, C., Feingold, G., Forster, P., Kerminen, V.-M., Kondo, Y., Liao, H., Lohmann, U., Rasch, P., Satheesh, S. K., Sherwood, S., Stevens, B., and Zhang, X. Y.: Clouds and Aerosols, in: Climate Change 2013 – The Physical Science Basis. Contribution of Working Group I to the Fifth Assessment Report of the Intergovernmental Panel on Climate Change, edited by: Stocker, T. F., Qin, D., Plattner, G.-K., Tignor, M., Allen, S. K., Boschung, J., Nauels, A., Xia, Y., Bex, V., and Midgley, P. M., Cambridge University Press, Cambridge, United Kingdom and New York, NY, USA, 571–658, https://doi.org/10.1017/CBO9781107415324.016, 2013.

Bunce, N. J., Liu, L., Zhu, J., and Lane, D. A.: Reaction of Naphthalene and Its Derivatives with Hydroxyl Radicals in the Gas Phase, Environ. Sci. Technol., 31, 2252–2259, https://doi.org/10.1021/es960813g, 1997.

Calvert, J. G., Atkinson, R., Becker, K. H., Kamens, R. M., Seinfeld, J. H., Wallington, T. J., and Yarwood, G.: The mechanisms of atmospheric oxidation of aromatic hydrocarbons, Oxford University Press, Oxford, 556 pp., https://doi.org/10.1093/oso/9780195146288.001.0001, 2002.

Chan, A. W. H., Kautzman, K. E., Chhabra, P. S., Surratt, J. D., Chan, M. N., Crounse, J. D., Kürten, A., Wennberg, P. O., Flagan, R. C., and Seinfeld, J. H.: Secondary organic aerosol formation from photooxidation of naphthalene and alkylnaphthalenes: implications for oxidation of intermediate volatility organic compounds (IVOCs), Atmos. Chem. Phys., 9, 3049–3060, https://doi.org/10.5194/acp-9-3049-2009, 2009.

Chen, C. L., Kacarab, M., Tang, P., and Cocker, D. R.: SOA formation from naphthalene, 1-methylnaphthalene, and 2-methylnaphthalene photooxidation, Atmos. Environ., 131, 424–433, https://doi.org/10.1016/j.atmosenv.2016.02.007, 2016.

Durant, J. L., Lafleur, A. L., Plummer, E. F., Taghizadeh, K., Busby, W. F., and Thilly, W. G.: Human Lymphoblast Mutagens in Urban Airborne Particles, Environ. Sci. Technol., 32, 1894–1906, https://doi.org/10.1021/es9706965, 1998.

Edwards, K. C., Klodt, A. L., Galeazzo, T., Schervish, M., Wei, J., Fang, T., Donahue, N. M., Aumont, B., Nizkorodov, S. A., and Shiraiwa, M.: Effects of Nitrogen Oxides on the Production of Reactive Oxygen Species and Environmentally Persistent Free Radicals from α-Pinene and Naphthalene Secondary Organic Aerosols, J. Phys. Chem. A, 126, 7361–7372, https://doi.org/10.1021/acs.jpca.2c05532, 2022.

Ensberg, J. J., Hayes, P. L., Jimenez, J. L., Gilman, J. B., Kuster, W. C., de Gouw, J. A., Holloway, J. S., Gordon, T. D., Jathar, S., Robinson, A. L., and Seinfeld, J. H.: Emission factor ratios, SOA mass yields, and the impact of vehicular emissions on SOA formation, Atmos. Chem. Phys., 14, 2383–2397, https://doi.org/10.5194/acp-14-2383-2014, 2014.

Fredenslund, A., Jones, R. L., and Prausnitz, J. M.: Group-contribution estimation of activity coefficients in nonideal liquid mixtures, AIChE J., 21, 1086–1099, https://doi.org/10.1002/aic.690210607, 1975.

Gelencsér, A., May, B., Simpson, D., Sánchez-Ochoa, A., Kasper-Giebl, A., Puxbaum, H., Caseiro, A., Pio, C., and Legrand, M.: Source apportionment of $PM_{2.5}$ organic aerosol over Europe: Primary/secondary, natural/anthropogenic, and fossil/biogenic origin, J. Geophys. Res., 112, D23S04, https://doi.org/10.1029/2006JD008094, 2007.

Glowacki, D. R., Wang, L., and Pilling, M. J.: Evidence of Formation of Bicyclic Species in the Early Stages of Atmospheric Benzene Oxidation, J. Phys. Chem. A, 113, 5385–5396, https://doi.org/10.1021/jp9001466, 2009.

Goliff, W. S., Stockwell, W. R., and Lawson, C. V.: The regional atmospheric chemistry mechanism, version 2, Atmos. Environ., 68, 174–185, https://doi.org/10.1016/j.atmosenv.2012.11.038, 2013.

Gupta, P., Harger, W. P., and Arey, J.: The contribution of nitro- and methylnitronaphthalenes to the vapor-phase mutagenic-

ity of ambient air samples, Atmos. Environ., 30, 3157–3166, https://doi.org/10.1016/1352-2310(96)00024-6, 1996.

Hallquist, M., Wenger, J. C., Baltensperger, U., Rudich, Y., Simpson, D., Claeys, M., Dommen, J., Donahue, N. M., George, C., Goldstein, A. H., Hamilton, J. F., Herrmann, H., Hoffmann, T., Iinuma, Y., Jang, M., Jenkin, M. E., Jimenez, J. L., Kiendler-Scharr, A., Maenhaut, W., McFiggans, G., Mentel, Th. F., Monod, A., Prévôt, A. S. H., Seinfeld, J. H., Surratt, J. D., Szmigielski, R., and Wildt, J.: The formation, properties and impact of secondary organic aerosol: current and emerging issues, Atmos. Chem. Phys., 9, 5155–5236, https://doi.org/10.5194/acp-9-5155-2009, 2009.

Helmig, D., Arey, J., Harger, W. P., Atkinson, R., and Lopez-Cancio, J.: Formation of mutagenic nitrodibenzopyranones and their occurrence in ambient air, Environ. Sci. Technol., 26, 622–624, https://doi.org/10.1021/es00027a028, 1992a.

Helmig, D., Lopez-Cancio, J., Arey, J., Harger, W. P., and Atkinson, R.: Quantification of ambient nitrodibenzopyranones: further evidence for atmospheric mutagen formation, Environ. Sci. Technol., 26, 2207–2213, https://doi.org/10.1021/es00035a020, 1992b.

Henze, D. K., Seinfeld, J. H., Ng, N. L., Kroll, J. H., Fu, T.-M., Jacob, D. J., and Heald, C. L.: Global modeling of secondary organic aerosol formation from aromatic hydrocarbons: high-vs. low-yield pathways, Atmos. Chem. Phys., 8, 2405–2420, https://doi.org/10.5194/acp-8-2405-2008, 2008.

Hu, J., Chen, Z., Qin, X., and Dong, P.: Reversible and irreversible gas–particle partitioning of dicarbonyl compounds observed in the real atmosphere, Atmos. Chem. Phys., 22, 6971–6987, https://doi.org/10.5194/acp-22-6971-2022, 2022.

Jenkin, M. E., Saunders, S. M., Wagner, V., and Pilling, M. J.: Protocol for the development of the Master Chemical Mechanism, MCM v3 (Part B): tropospheric degradation of aromatic volatile organic compounds, Atmos. Chem. Phys., 3, 181–193, https://doi.org/10.5194/acp-3-181-2003, 2003.

Jenkin, M. E., Valorso, R., Aumont, B., Rickard, A. R., and Wallington, T. J.: Estimation of rate coefficients and branching ratios for gas-phase reactions of OH with aliphatic organic compounds for use in automated mechanism construction, Atmos. Chem. Phys., 18, 9297–9328, https://doi.org/10.5194/acp-18-9297-2018, 2018a.

Jenkin, M. E., Valorso, R., Aumont, B., Rickard, A. R., and Wallington, T. J.: Estimation of rate coefficients and branching ratios for gas-phase reactions of OH with aromatic organic compounds for use in automated mechanism construction, Atmos. Chem. Phys., 18, 9329–9349, https://doi.org/10.5194/acp-18-9329-2018, 2018b.

Jenkin, M. E., Valorso, R., Aumont, B., and Rickard, A. R.: Estimation of rate coefficients and branching ratios for reactions of organic peroxy radicals for use in automated mechanism construction, Atmos. Chem. Phys., 19, 7691–7717, https://doi.org/10.5194/acp-19-7691-2019, 2019.

Jimenez, J. L., Canagaratna, M. R., Donahue, N. M., Prevot, A. S. H., Zhang, Q., Kroll, J. H., DeCarlo, P. F., Allan, J. D., Coe, H., Ng, N. L., Aiken, A. C., Docherty, K. S., Ulbrich, I. M., Grieshop, A. P., Robinson, A. L., Duplissy, J., Smith, J. D., Wilson, K. R., Lanz, V. A., Hueglin, C., Sun, Y. L., Tian, J., Laaksonen, A., Raatikainen, T., Rautiainen, J., Vaattovaara, P., Ehn, M., Kulmala, M., Tomlinson, J. M., Collins, D. R., Cubison, M. J., Dunlea, J., Huffman, J. A., Onasch, T. B., Alfarra, M. R., Williams, P. I., Bower, K., Kondo, Y., Schneider, J., Drewnick, F., Borrmann, S., Weimer, S., Demerjian, K., Salcedo, D., Cottrell, L., Griffin, R., Takami, A., Miyoshi, T., Hatakeyama, S., Shimono, A., Sun, J. Y., Zhang, Y. M., Dzepina, K., Kimmel, J. R., Sueper, D., Jayne, J. T., Herndon, S. C., Trimborn, A. M., Williams, L. R., Wood, E. C., Middlebrook, A. M., Kolb, C. E., Baltensperger, U., and Worsnop, D. R.: Evolution of Organic Aerosols in the Atmosphere, Science, 326, 1525–1529, https://doi.org/10.1126/science.1180353, 2009.

Josephy, P. D. and Mannervik, B.: Molecular toxicology, Oxford University Press, Oxford, 608 pp., ISBN 9780195176209, 2006.

Kautzman, K. E., Surratt, J. D., Chan, M. N., Chan, A. W. H., Hersey, S. P., Chhabra, P. S., Dalleska, N. F., Wennberg, P. O., Flagan, R. C., and Seinfeld, J. H.: Chemical composition of gas- and aerosol-phase products from the photooxidation of naphthalene, J. Phys. Chem. A, 114, 913–934, https://doi.org/10.1021/jp908530s, 2010.

Kerdouci, J., Picquet-Varrault, B., and Doussin, J.: Prediction of Rate Constants for Gas-Phase Reactions of Nitrate Radical with Organic Compounds: A New Structure–Activity Relationship, Chem. Phys. Chem., 11, 3909–3920, https://doi.org/10.1002/cphc.201000673, 2010.

Kerdouci, J., Picquet-Varrault, B., and Doussin, J.-F.: Structure–activity relationship for the gas-phase reactions of NO_3 radical with organic compounds: Update and extension to aldehydes, Atmos. Environ., 84, 363–372, https://doi.org/10.1016/j.atmosenv.2013.11.024, 2014.

Keyte, I. J., Albinet, A., and Harrison, R. M.: On-road traffic emissions of polycyclic aromatic hydrocarbons and their oxy- and nitro- derivative compounds measured in road tunnel environments, Sci. Total Environ., 566–567, 1131–1142, https://doi.org/10.1016/j.scitotenv.2016.05.152, 2016.

Kroll, J. H. and Seinfeld, J. H.: Chemistry of secondary organic aerosol: Formation and evolution of low-volatility organics in the atmosphere, Atmos. Environ., 42, 3593–3624, https://doi.org/10.1016/j.atmosenv.2008.01.003, 2008.

Lannuque, V., D'anna, B., Couvidat, F., Valorso, R., and Sartelet, K.: Improvement in modeling of oh and ho2 radical concentrations during toluene and xylene oxidation with racm2 using mcm/gecko-a, Atmosphere, 12, 732, https://doi.org/10.3390/atmos12060732, 2021.

Lannuque, V., D'Anna, B., Kostenidou, E., Couvidat, F., Martinez-Valiente, A., Eichler, P., Wisthaler, A., Müller, M., Temime-Roussel, B., Valorso, R., and Sartelet, K.: Gas–particle partitioning of toluene oxidation products: an experimental and modeling study, Atmos. Chem. Phys., 23, 15537–15560, https://doi.org/10.5194/acp-23-15537-2023, 2023.

Lim, C. C., Hayes, R. B., Ahn, J., Shao, Y., Silverman, D. T., Jones, R. R., Garcia, C., and Thurston, G. D.: Association between long-term exposure to ambient air pollution and diabetes mortality in the US, Environ. Res., 165, 330–336, https://doi.org/10.1016/j.envres.2018.04.011, 2018.

Lim, S. S., Vos, T., Flaxman, A. D., Danaei, G., Shibuya, K., Adair-Rohani, H., AlMazroa, M. A., Amann, M., Anderson, H. R., Andrews, K. G., Aryee, M., Atkinson, C., Bacchus, L. J., Bahalim, A. N., Balakrishnan, K., Balmes, J., Barker-Collo, S., Baxter, A., Bell, M. L., Blore, J. D., Blyth, F., Bonner, C., Borges, G., Bourne, R., Boussinesq, M., Brauer, M., Brooks, P., Bruce, N.

G., Brunekreef, B., Bryan-Hancock, C., Bucello, C., Buchbinder, R., Bull, F., Burnett, R. T., Byers, T. E., Calabria, B., Carapetis, J., Carnahan, E., Chafe, Z., Charlson, F., Chen, H., Chen, J. S., Cheng, A. T.-A., Child, J. C., Cohen, A., Colson, K. E., Cowie, B. C., Darby, S., Darling, S., Davis, A., Degenhardt, L., Dentener, F., Des Jarlais, D. C., Devries, K., Dherani, M., Ding, E. L., Dorsey, E. R., Driscoll, T., Edmond, K., Ali, S. E., Engell, R. E., Erwin, P. J., Fahimi, S., Falder, G., Farzadfar, F., Ferrari, A., Finucane, M. M., Flaxman, S., Fowkes, F. G. R., Freedman, G., Freeman, M. K., Gakidou, E., Ghosh, S., Giovannucci, E., Gmel, G., Graham, K., Grainger, R., Grant, B., Gunnell, D., Gutierrez, H. R., Hall, W., Hoek, H. W., Hogan, A., Hosgood, H. D., Hoy, D., Hu, H., Hubbell, B. J., Hutchings, S. J., Ibeanusi, S. E., Jacklyn, G. L., Jasrasaria, R., Jonas, J. B., Kan, H., Kanis, J. A., Kassebaum, N., Kawakami, N., Khang, Y.-H., Khatibzadeh, S., Khoo, J.-P., Kok, C., Laden, F., Lalloo, R., Lan, Q., Lathlean, T., Leasher, J., Leigh, J., Li, Y., Lin, J., Lipshultz, S., London, S., Lozano, R., Lu, Y., Mak, J., Malekzadeh, R., Mallinger, L., Marcenes, W., March, L., Marks, R., Martin, R., McGale, P., McGrath, J., Mehta, S., Mensah, G., Merriman, T., Micha, R., Michaud, C., Mishra, V., Hanafiah, K., Mokdad, A., Morawska, L., Mozaffarian, D., Murphy, T., Naghavi, M., Neal, B., Nelson, P., Nolla, J., Norman, R., Olives, C., Omer, S., Orchard, J., Osborne, R., Ostro, B., Page, A., Pandey, K., Parry, C., Passmore, E., Patra, J., Pearce, N., Pelizzari, P., Petzold, M., Phillips, M., Pope, D., Pope, C., Powles, J., Rao, M., Razavi, H., Rehfuess, E., Rehm, J., Ritz, B., Rivara, F., Roberts, T., Robinson, C., Rodriguez-Portales, J., Romieu, I., Room, R., Rosenfeld, L., Roy, A., Rushton, L., Salomon, J., Sampson, U., Sanchez-Riera, L., Sanman, E., Sapkota, A., Seedat, S., Shi, P., Shield, K., Shivakoti, R., Singh, G., Sleet, D., Smith, E., Smith, K., Stapelberg, N., Steenland, K., Stöckl, H., Stovner, L., Straif, K., Straney, L., Thurston, G., Tran, J., Van Dingenen, R., Van Donkelaar, A., Veerman, J., Vijayakumar, L., Weintraub, R., Weissman, M., White, R., Whiteford, H., Wiersma, S., Wilkinson, J., Williams, H., Williams, W., Wilson, N., Woolf, A., Yip, P., Zielinski, J., Lopez, A., Murray, C., and Ezzati, M.: A comparative risk assessment of burden of disease and injury attributable to 67 risk factors and risk factor clusters in 21 regions, 1990–2010: a systematic analysis for the Global Burden of Disease Study 2010, Lancet, 380, 2224–2260, https://doi.org/10.1016/S0140-6736(12)61766-8, 2012.

Majdi, M., Sartelet, K., Lanzafame, G. M., Couvidat, F., Kim, Y., Chrit, M., and Turquety, S.: Precursors and formation of secondary organic aerosols from wildfires in the Euro-Mediterranean region, Atmos. Chem. Phys., 19, 5543–5569, https://doi.org/10.5194/acp-19-5543-2019, 2019.

Malley, C. S., Kuylenstierna, J. C. I., Vallack, H. W., Henze, D. K., Blencowe, H., and Ashmore, M. R.: Preterm birth associated with maternal fine particulate matter exposure: A global, regional and national assessment, Environ. Int., 101, 173–182, https://doi.org/10.1016/j.envint.2017.01.023, 2017.

Martinet, S., Liu, Y., Louis, C., Tassel, P., Perret, P., Chaumond, A., and André, M.: Euro 6 Unregulated Pollutant Characterization and Statistical Analysis of After-Treatment Device and Driving-Condition Impact on Recent Passenger-Car Emissions, Environ. Sci. Technol., 51, 5847–5855, https://doi.org/10.1021/acs.est.7b00481, 2017.

Martinez, A.: Contribution of volatile organic compounds (VOCs) from vehicle emissions to secondary organic aerosol (SOA) and urban pollution, Université de Lyon, https://theses.hal.science/tel-03184951 (last access: 31 July 2024), 2019.

Mastral, A. M. and Callén, M. S.: A Review on Polycyclic Aromatic Hydrocarbon (PAH) Emissions from Energy Generation, Environ. Sci. Technol., 34, 3051–3057, https://doi.org/10.1021/es001028d, 2000.

Mihele, C. M., Wiebe, H. A., and Lane, D. A.: Particle Formation and Gas/Particle Partition Measurements of the Products of the Naphthalene-OH Radical Reaction in a Smog Chamber, Polycycl. Aromat. Compd., 22, 729–736, https://doi.org/10.1080/10406630290103889, 2002.

Mousavipour, S. H. and Homayoon, Z.: Multichannel RRKM-TST and CVT rate constant calculations for reactions of CH_2OH or CH_3O with HO_2, J. Phys. Chem. A, 115, 3291–3300, https://doi.org/10.1021/jp112081r, 2011.

Müller, M., Graus, M., Wisthaler, A., Hansel, A., Metzger, A., Dommen, J., and Baltensperger, U.: Analysis of high mass resolution PTR-TOF mass spectra from 1,3,5-trimethylbenzene (TMB) environmental chamber experiments, Atmos. Chem. Phys., 12, 829–843, https://doi.org/10.5194/acp-12-829-2012, 2012.

Muñoz, M., Haag, R., Zeyer, K., Mohn, J., Comte, P., Czerwinski, J., and Heeb, N. V: Effects of Four Prototype Gasoline Particle Filters (GPFs) on Nanoparticle and Genotoxic PAH Emissions of a Gasoline Direct Injection (GDI) Vehicle, Environ. Sci. Technol., 52, 10709–10718, https://doi.org/10.1021/acs.est.8b03125, 2018.

Nannoolal, Y., Rarey, J., Ramjugernath, D., and Cordes, W.: Estimation of pure component properties: Part 1. Estimation of the normal boiling point of non-electrolyte organic compounds via group contributions and group interactions, Fluid Phase Equilib., 226, 45–63, https://doi.org/10.1016/j.fluid.2004.09.001, 2004.

Nannoolal, Y., Rarey, J., and Ramjugernath, D.: Estimation of pure component properties: Part 3. Estimation of the vapor pressure of non-electrolyte organic compounds via group contributions and group interactions, Fluid Phase Equilib., 269, 117–133, https://doi.org/10.1016/j.fluid.2008.04.020, 2008.

Nishino, N., Atkinson, R., and Arey, J.: Formation of Nitro Products from the Gas-Phase OH Radical-Initiated Reactions of Toluene, Naphthalene, and Biphenyl: Effect of NO_2 Concentration, Environ. Sci. Technol., 42, 9203–9209, https://doi.org/10.1021/es802046m, 2008.

Nojima, K. and Kanno, S.: Studies on photochemistry of aromatic hydrocarbons IV. Mechanism of formation of nitrophenols by the photochemical reaction of benzene and toluene with nitrogen oxides in air, Chemosphere, 6, 371–376, https://doi.org/10.1016/0045-6535(77)90102-3, 1977.

Olivella, S., Solé, A., and Bofill, J. M.: Theoretical mechanistic study of the oxidative degradation of benzene in the troposphere: reaction of benzene-ho radical adduct with o_2, J. Chem. Theory Comput., 5, 1607–1623, https://doi.org/10.1021/ct900082g, 2009.

Phousongphouang, P. T. and Arey, J.: Rate Constants for the Gas-Phase Reactions of a Series of Alkylnaphthalenes with the OH Radical, Environ. Sci. Technol., 36, 1947–1952, https://doi.org/10.1021/es011434c, 2002.

Phousongphouang, P. T. and Arey, J.: Rate constants for the gas-phase reactions of a series of alkylnaphthalenes with the nitrate radical, Environ. Sci. Technol., 37, 308–313, https://doi.org/10.1021/es026015+, 2003a.

Phousongphouang, P. T. and Arey, J.: Rate constants for the photolysis of the nitronaphthalenes and methylnitronaphthalenes, J. Photochem. Photobiol. A Chem., 157, 301–309, https://doi.org/10.1016/S1010-6030(03)00072-8, 2003b.

Platz, J., Nielsen, O. J., Wallington, T. J., Ball, J. C., Hurley, M. D., Straccia, A. M., Schneider, W. F., and Sehested, J.: Atmospheric chemistry of the phenoxy radical, $C_6H_5O(\bullet)$: UV spectrum and kinetics of its reaction with NO, NO_2, and O_2, J. Phys. Chem. A, 102, 7964–7974, https://doi.org/10.1021/jp982221l, 1998.

Ravindra, K., Sokhi, R., and Vangrieken, R.: Atmospheric polycyclic aromatic hydrocarbons: Source attribution, emission factors and regulation, Atmos. Environ., 42, 2895–2921, https://doi.org/10.1016/j.atmosenv.2007.12.010, 2008.

Robinson, A. L., Donahue, N. M., Shrivastava, M. K., Weitkamp, E. A., Sage, A. M., Grieshop, A. P., Lane, T. E., Pierce, J. R., and Pandis, S. N.: Rethinking Organic Aerosols: Semivolatile Emissions and Photochemical Aging, Science, 315, 1259–1262, https://doi.org/10.1126/science.1133061, 2007.

Roueintan, M. M., Cho, J., and Li, Z.: Kinetics Investigation of Reaction of Naphthalene with OH Radicals at 1–3 Torr and 240–340 K, Int. J. Chem. Kinet., 46, 578–586, https://doi.org/10.1002/kin.20870, 2014.

Sartelet, K., Couvidat, F., Wang, Z., Flageul, C., and Kim, Y.: SSH-Aerosol v1.1: A Modular Box Model to Simulate the Evolution of Primary and Secondary Aerosols, Atmosphere, 11, 525, https://doi.org/10.3390/atmos11050525, 2020.

Sartelet, K., Couvidat, F., Wang, Z., Lannuque, V., Flageul, C., and Kim, Y.: SSH-aerosol: a modular box model to simulate the evolution of primary and secondary aerosols (1.3), Zenodo [code], https://doi.org/10.5281/zenodo.10159225, 2022.

Sasaki, J., Arey, J., and Harger, W. P.: Formation of Mutagens from the Photooxidations of 2-4-Ring PAH, Environ. Sci. Technol., 29, 1324–1335, https://doi.org/10.1021/es00005a027, 1995.

Sasaki, J. C., Arey, J., Eastmond, D. A., Parks, K. K., and Grosovsky, A. J.: Genotoxicity induced in human lymphoblasts by atmospheric reaction products of naphthalene and phenanthrene, Mutat. Res. Toxicol. Environ. Mutagen., 393, 23–35, https://doi.org/10.1016/S1383-5718(97)00083-1, 1997.

Schauer, J. J., Kleeman, M. J., Cass, G. R., and Simoneit, B. R. T.: Measurement of Emissions from Air Pollution Sources. 1. C1 through C29 Organic Compounds from Meat Charbroiling, Environ. Sci. Technol., 33, 1566–1577, https://doi.org/10.1021/es980076j, 1999a.

Schauer, J. J., Kleeman, M. J., Cass, G. R., and Simoneit, B. R. T.: Measurement of emissions from air pollution sources. 2. C1 through C30 organic compounds from medium duty diesel trucks, Environ. Sci. Technol., 33, 1578–1587, https://doi.org/10.1021/es980081n, 1999b.

Schauer, J. J., Kleeman, M. J., Cass, G. R., and Simoneit, B. R. T.: Measurement of Emissions from Air Pollution Sources. 3. C1−C29 Organic Compounds from Fireplace Combustion of Wood, Environ. Sci. Technol., 35, 1716–1728, https://doi.org/10.1021/es001331e, 2001.

Schauer, J. J., Kleeman, M. J., Cass, G. R., and Simoneit, B. R. T.: Measurement of Emissions from Air Pollution Sources. 4. C1-C27 Organic Compounds from Cooking with Seed Oils, Environ. Sci. Technol., 36, 567–575, https://doi.org/10.1021/es002053m, 2002a.

Schauer, J. J., Kleeman, M. J., Cass, G. R., and Simoneit, B. R. T.: Measurement of emissions from air pollution sources. 5. C1-C32 organic compounds from gasoline-powered motor vehicles., Environ. Sci. Technol., 36, 1169–1180, https://doi.org/10.1021/es0108077, 2002b.

Seigneur, C.: Air Pollution, Cambridge University Press, https://doi.org/10.1017/9781108674614, 2019.

Seinfeld, J. H. and Pankow, J. F.: Organic Atmospheric Particulate Material, Annu. Rev. Phys. Chem., 54, 121–140, https://doi.org/10.1146/annurev.physchem.54.011002.103756, 2003.

Shiroudi, A., Deleuze, M. S., and Canneaux, S.: Theoretical Study of the Oxidation Mechanisms of Naphthalene Initiated by Hydroxyl Radicals: The OH-Addition Pathway, J. Phys. Chem. A, 118, 4593–4610, https://doi.org/10.1021/jp411327e, 2014.

Tao, Z. and Li, Z.: A kinetics study on reactions of C_6H_5O with C_6H_5O and O_3 at 298 k, Int. J. Chem. Kinet., 31, 65–72, https://doi.org/10.1002/(SICI)1097-4601(1999)31:1<65::AID-KIN8>3.0.CO;2-J, 1999.

Tokiwa, H., Ohnishi, Y., and Rosenkranz, H. S.: Mutagenicity and Carcinogenicity of Nitroarenes and Their Sources in the Environment, CRC Crit. Rev. Toxicol., 17, 23–58, https://doi.org/10.3109/10408448609037070, 1986.

Vereecken, L. and Peeters, J.: Decomposition of substituted alkoxy radicals – part I: a generalized structure–activity relationship for reaction barrier heights, Phys. Chem. Chem. Phys., 11, 9062, https://doi.org/10.1039/b909712k, 2009.

Vereecken, L. and Peeters, J.: A structure-activity relationship for the rate coefficient of H-migration in substituted alkoxy radicals, Phys. Chem. Chem. Phys., 12, 12608–12620, https://doi.org/10.1039/c0cp00387e, 2010.

Wang, L., Atkinson, R., and Arey, J.: Dicarbonyl Products of the OH Radical-Initiated Reactions of Naphthalene and the C1- and C2-Alkylnaphthalenes, Environ. Sci. Technol., 41, 2803–2810, https://doi.org/10.1021/es0628102, 2007.

Wang, S., Ye, J., Soong, R., Wu, B., Yu, L., Simpson, A. J., and Chan, A. W. H.: Relationship between chemical composition and oxidative potential of secondary organic aerosol from polycyclic aromatic hydrocarbons, Atmos. Chem. Phys., 18, 3987–4003, https://doi.org/10.5194/acp-18-3987-2018, 2018.

Yuan, B., Hu, W. W., Shao, M., Wang, M., Chen, W. T., Lu, S. H., Zeng, L. M., and Hu, M.: VOC emissions, evolutions and contributions to SOA formation at a receptor site in eastern China, Atmos. Chem. Phys., 13, 8815–8832, https://doi.org/10.5194/acp-13-8815-2013, 2013.

Zhang, Q., Jimenez, J. L., Canagaratna, M. R., Allan, J. D., Coe, H., Ulbrich, I., Alfarra, M. R., Takami, A., Middlebrook, A. M., Sun, Y. L., Dzepina, K., Dunlea, E., Docherty, K., DeCarlo, P. F., Salcedo, D., Onasch, T., Jayne, J. T., Miyoshi, T., Shimono, A., Hatakeyama, S., Takegawa, N., Kondo, Y., Schneider, J., Drewnick, F., Borrmann, S., Weimer, S., Demerjian, K., Williams, P., Bower, K., Bahreini, R., Cottrell, L., Griffin, R. J., Rautiainen, J., Sun, J. Y., Zhang, Y. M., and Worsnop, D. R.: Ubiquity and dominance of oxygenated species in organic aerosols in anthropogenically-influenced Northern

Hemisphere midlatitudes, Geophys. Res. Lett., 34, L13801, https://doi.org/10.1029/2007GL029979, 2007.

Zhang, Z., Lin, L., and Wang, L.: Atmospheric oxidation mechanism of naphthalene initiated by OH radical. A theoretical study, Phys. Chem. Chem. Phys., 14, 2645–2650, https://doi.org/10.1039/C2CP23271E, 2012.

Zuend, A., Marcolli, C., Luo, B. P., and Peter, T.: A thermodynamic model of mixed organic-inorganic aerosols to predict activity coefficients, Atmos. Chem. Phys., 8, 4559–4593, https://doi.org/10.5194/acp-8-4559-2008, 2008.